Electrochimica Acta 212 (2016) 921–928

Contents lists available at ScienceDirect

Electrochimica Acta

journal homepage: www.elsevier.com/locate/electacta

Electrochemical Characterization of Natural Chalcopyrite Dissolution in Sulfuric Acid Solution in Presence of Peroxydisulfate

Ali Rafsanjani-Abbasi[a], Ali Davoodi[b,*]

[a] Materials and Polymers Engineering Department, Faculty of Engineering, Hakim Sabzevari University, Sabzevar, Iran
[b] Materials and Metallurgical Engineering Department, Faculty of Engineering, Ferdowsi University of Mashhad, Mashhad, Iran

ARTICLE INFO

Article history:
Received 26 April 2016
Received in revised form 11 July 2016
Accepted 12 July 2016
Available online 12 July 2016

Keywords:
Chalcopyrite
Hydrometallurgy
Peroxydisulfate
AFM
EIS

ABSTRACT

In this study, the effect of peroxydisulfate ion on electrochemical behavior of natural chalcopyrite in 0.5 M H_2SO_4 was investigated by means of AC/DC electrochemical tests and atomic force microscopy (AFM). Regarding potentiodynamic polarization (PDP) and electrochemical impedance spectroscopy (EIS), increase in peroxydisulfate ion concentration accelerates the electrochemical dissolution of the chalcopyrite electrode. Also, Mott-Schottky measurements proved that peroxydisulfate ion decreases n-type semiconducting properties of the chalcopyrite passive layer. Finally, atomic force microscopy showed directly that in presence of peroxydisulfate ion, chalcopyrite more severely corrodes compared with the blank sulfuric solution.

1. Introduction

Chalcopyrite ($CuFeS_2$) is the most important and abundant copper-bearing mineral in the earth's crust. About 20% of primary copper annual production comes from hydrometallurgical technologies [1]. Hydrometallurgy is preferred as an alternative process route for traditional pyrometallurgy, on the basis of environmental and economic issues [2]. High energy consumption and production of dust, toxic gases and trace metals specifically arsenic are causes for environmental concerns about pyrometallurgy. Alternatively, hydrometallurgical copper extraction processes have an ability to deal with low capacity operations and low grade minerals [3]. Refractory nature of chalcopyrite in hydrometallurgical processes is the most important reason for low contribution of hydrometallurgical copper production despite its superiority. The inhibition of chalcopyrite dissolution is caused by an insoluble passive layer formed on the surface of the mineral [4].

Chalcopyrite is a semiconducting material and its dissolution is essentially considered as an electrochemical process. The dissolution of chalcopyrite can be looked upon as an electrochemical reaction with cathodic reduction of oxidizing agent and anodic oxidation of the metal sulfide. So the electrochemical techniques are very helpful to have a mechanistic kinetic study on hydrometallurgy of copper [5]. Electrochemical investigations on chalcopyrite electrode characterize surface properties and sequence of surface layers formation. Traditional cyclic voltammetry (CV) method was often used to explore intermediate compounds during electrochemical dissolution of chalcopyrite [6,7]. Also, studies by electrochemical impedance spectroscopy (EIS) have been conducted to investigate active-passive behavior of chalcopyrite and heterogeneity of the passive layer [8–10]. Mott-Schottky analysis is another in-situ technique which has been utilized to study chalcopyrite semiconducting properties and electrode/electrolyte interface [11,12]. In general, in-situ electrochemical techniques are able to provide comprehensive information about dissolution mechanism of chalcopyrite. In addition, sensitive surface analysis methods such as X-ray photoelectron spectroscopy (XPS), Raman spectroscopy and scanning probe microscopy (SPM) are able to provide evidences for reliability of electrochemical results. Understanding of electrochemical dissolution behavior and surface chemistry of chalcopyrite represents important scientific considerations in both flotation and hydrometallurgical extraction [13–16].

Many methods have been developed to overcome chalcopyrite passive layer and to enhance the dissolution of chalcopyrite using different oxidants and additives. Ferric ion is one of the most important oxidants in hydrometallurgy and ferric assisted leaching of chalcopyrite in sulfuric media has been widely studied [17–19]. Hydrogen peroxide, ozone, dichromate and chlorate are another oxidants which have been used for oxidizing chalcopyrite in sulfuric acid media [20–23]. Most of the above mentioned oxidants

* Corresponding author.
E-mail addresses: a.davodi@um.ac.ir, adavoodi@kth.se, davoodiali@gmail.com (A. Davoodi).

http://dx.doi.org/10.1016/j.electacta.2016.07.061
0013-4686/

are usually not available near the mines naturally or need expensive and infrastructure facilities for developing to industrial scale. In addition, an ideal oxidant for leaching of chalcopyrite should be applicable for heap leaching at atmospheric pressure while some oxidants are only efficient in tank and high pressure leaching.

Peroxydisulfate is a very strong oxidizing agent which has an ability to be made from sulfuric acid using an electrochemical cell at low energy cost of 0.2 $ per kilogram [19,24]. Also, peroxydisulfate is not categorized in environmental toxics according to globally harmonized system (GHS) of classification and labelling of chemicals [25]. Peroxydisulfate concentrations up to 10 g/L do not affect the indigenous microorganisms and its effects on soil microorganisms are less damaging than those of Fenton's reagent and hydrogen peroxide [26]. Peroxydisulfate is a stronger oxidizer than hydrogen peroxide, permanganate, ozone and dichromate with a standard reduction potential of 2.123 V [27]:

$$S_2O_8^{2-} + 2H^+ + 2e^- \leftrightarrows 2HSO_4^- \quad (1)$$

Also, peroxydisulfate could be decomposed into two radicals with a standard reduction potential of 2.6 V:

$$S_2O_8^{2-} + \text{initiator} \leftrightarrows 2SO4^{-\bullet} \quad (2)$$

Regarding unique features of peroxydisulfate, Dakubo et al. used this oxidizing agent for the first time to enhance the leaching ability of copper from chalcopyrite in sulfuric acid media at pH 2. The focus of their study was on kinetic parameters of copper leaching such as reactor shape, ore grade, dissolved oxygen and particle size but a comprehensive electrochemical study is missing [28]. In this research, we are trying to study the electrochemical behavior of chalcopyrite to contribute to a deeper understanding of the mechanisms of chalcopyrite electrochemical dissolution. In addition, atomic force microscopy was used in a novel electrochemical test configuration to investigate surface changes during different conditions of electrochemical dissolution.

2. Experimental procedure

The chalcopyrite sample used in this study was a high purity natural polycrystalline mineral originating from Sarcheshmeh copper mine, Kerman, Iran. Mineralogical analysis and chemical composition of the sample was investigated by optical microscopy, X-ray diffraction (XRD) and X-ray fluorescence (XRF). The XRF semi-quantitative results showed that the chalcopyrite contained 33.05% Cu, 33.03% S, 30.21% Fe, 2.48% SiO_2, 0.65% Al_2O_3, 0.11% CaO,0.10% K_2O and 0.03% Mo. Mineralogical analysis is calculated based on the chemical analysis and knowledge from optical microscopy of the mineralogical phases present in the sample. The phase analysis of the chalcopyrite ore is shown in Table 1.

A massive specimen of chalcopyrite was cut into cubic shapes using precision cutter machine. Electrical connection was made with a copper wire at the bottom of the cubic specimen by conductive silver glue. Then, the whole assembly mounted in a low viscosity epoxy resin leaving 0.6 cm^2 exposed surface area. Prior to each electrochemical measurement, the chalcopyrite surface was wet-ground to 1500-grit finish by abrasive silicon carbide paper, washed in deionized water and dried with hot air. The fresh

Table 1
Composition of natural chalcopyrite ore received from Sarcheshemeh copper mine, Iran.

Mineral	Chalcopyrite	Pyrite	Molybdenite	Limonite	Sphalerite
Composition (wt %)	94.974	2.635	0.047	0.109	0.125

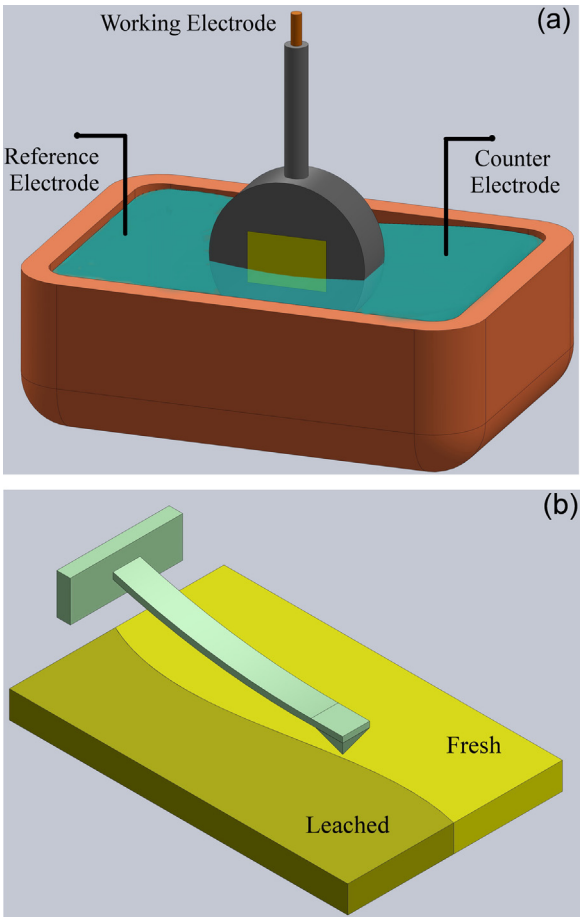

Fig. 1. Electrochemical test configuration for atomic force microscopy.

electrolyte solution containing 0.5 M H_2SO_4, either without peroxydisulfate, or in presence of 0.001, 0.01 and 0.1 M peroxydisulfate concentrations added as $K_2S_2O_8$ salt, was purchased and then prepared from Merck reagents and deionized water for each test. All of the experiments were conducted at ambient temperature.

The electrochemical measurements were performed three times to ensure the reproducibility in the following sequence:

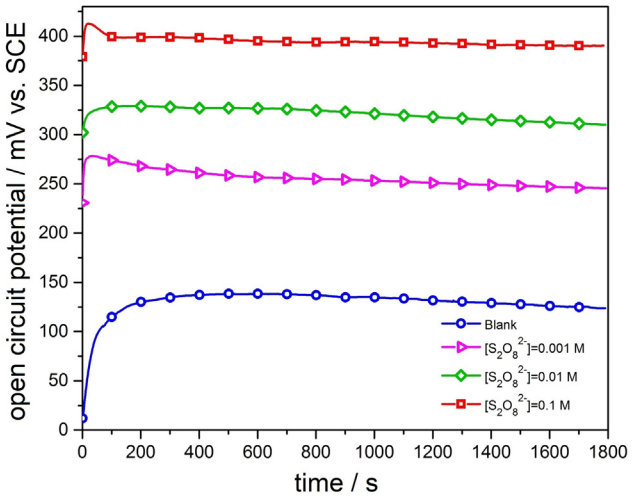

Fig. 2. Open circuit potential of chalcopyrite electrode for different concentrations of peroxydisulfate in 0.5 M H_2SO_4.

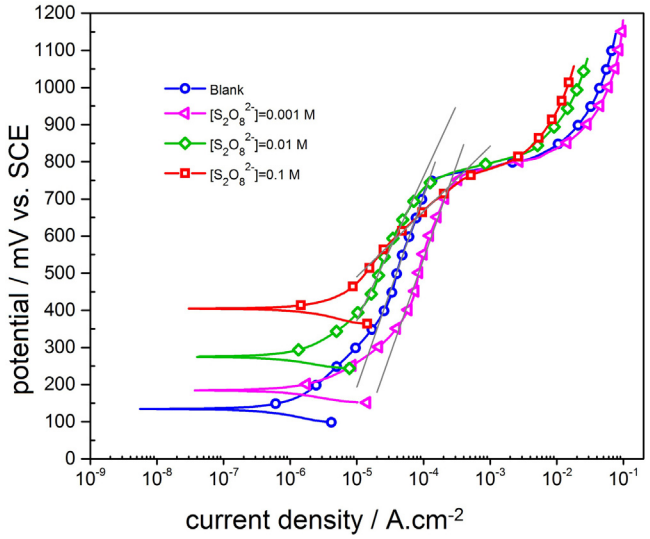

Fig. 3. Potentiodynamic polarization of chalcopyrite electrode for different concentrations of peroxydisulfate in 0.5 M H_2SO_4.

i 1800 seconds open circuit potential (OCP) recording.
ii Potentiodynamic polarization (PDP) by changing the electrode potential from −50 mV to 1000 mV versus OCP with scan rate of 0.5 mV/s.
iii Electrochemical impedance spectroscopy (EIS) measurement at OCP in the frequency range of 0.01 Hz to 10 kHz by applying sinusoidal excitation signal of ±10 mV.
iv Mott-Schottky analysis at 1 kHz frequency in the potential range of 300 mV to 900 mV vs. saturated calomel electrode (SCE) with amplitude of ±10 mV.

All electrochemical measurements were conducted by means of CompactStat Ivium potentiostat instrument, using saturated calomel electrode and platinum wire as reference electrode and counter electrode, respectively. The EIS equivalent circuit components are extracted using EIS spectrum analyzer.

Finally, the topography images were taken using a commercial Solver Next model AFM instrument (NT-MDT Co.). All scanning probe microscopies were performed in the air at ambient temperature with relative humidity of 25 ± 5%. Topographical scanning were performed with a pixel resolution of 256 × 256 and scan frequency rate of 0.4 Hz. A doped silicon pyramid was used as an AFM tip. Before scanning probe microscopy, the surface of chalcopyrite electrode was polished and uniform gold-color surface was achieved using alumina suspension (from 0.3 to 0.05 micrometer). Then, a novel electrochemical test configuration was employed to study the chalcopyrite surface changes during electrochemical dissolution. In this regard, a chalcopyrite electrode was held in a solution in a manner that approximately half of the surface area of the electrode was exposed to the solution and the other half was remained in air. After applying constant potential of 720 mV and 820 mV (vs. SCE) to the chalcopyrite electrode for 4 hours, scanning probe microscopy was conducted exactly on the border of leached and fresh surface (Fig. 1). Following the above procedure, it was expected that two regions could be observed at the same AFM image.

3. Results and discussion

3.1. Open circuit potential (OCP)

In order to reach a rest potential before electrochemical experiments, variations in the OCP of the chalcopyrite electrode in 0.5 M sulfuric acid with different concentrations of peroxydisulfate ion was monitored and the results are shown in Fig. 2. As can be seen, the OCP of the chalcopyrite electrode shows a gradual increase at the beginning which is an evidence for development of the passive layer, particularly on the sample immersed in blank sulfuric acid. Fig. 2 also illustrates that the rest potential stabilized almost after about 300 seconds. Also, the OCP shifts to more positive values by increasing peroxydisulfate ion concentration up to ca. 400 mV vs. SCE due to high oxidizing power of peroxydisulfate on the chalcopyrite electrode.

3.2. Potentiodynamic polarization (PDP)

Fig. 3 represents potentiodynamic polarization curves for the chalcopyrite electrode in 0.5 M H_2SO_4 in absence and presence of peroxydisulfate ion. As can be seen, the polarization curves do not show complete linear Tafel region and accurate evaluation of Tafel slopes using Tafel extrapolation is not possible. Therefore, some authors have proposed similar methods using software analysis which are able to calculate Tafel parameters with acceptable deviation less than 10% from other regular methods of corrosion rate determination [29,30]. Electrochemical parameters of the chalcopyrite corrosion including corrosion potential (E_{corr}), corrosion current density (j_{corr}) and anodic Tafel slope (β_a) have been calculated using model analysis of Ivium software and listed in Table 2 where plus and minus sign refers to quantitative information obtained from repetition of the experiment.

Anodic polarization curves show active and pseudo-passive regions followed by a transition to transpassive behavior. At low positive over potentials, active dissolution of chalcopyrite could be observed during the anodic polarization for all solutions. By assessing Table 2, a considerable increase in the corrosion current density of chalcopyrite up to less than one decay can be observed in presence of peroxydisulfate ion proving that peroxydisulfate plays an important oxidation role for dissolution of chalocpyrite. Also, a significant change in the anodic Tafel slope was observed by increasing the oxidizer concentration.

At higher anodic over potentials, the chalcopyrite has a pseudo-passive behavior. The slope of this pseudo-passive region was calculated using linear fitting. As can be seen in Fig. 3, the pseudo-passive region of the curves has a linear behavior and the slope of this line has decreased at higher concentrations of the oxidizer. In other words, variations in current density of chalcopyrite in a constant range of over potentials are greater at higher concentrations of the oxidizer. Therefore, presence of peroxydisulfate ion has deteriorated the metal-deficient passive layer on the chalcopyrite surface partially. After pseudo-passive range, a rapid

Table 2
Electrochemical potential polarization parameters for chalcopyrite in the absence and presence of peroxydisulfate.

	E_{corr} (mV)	j_{corr} (μA cm^{-2})	Tafel anodic slope (β_a) (mV dec^{-1})	pseudo-passive linear slope (β_{pp}) (mV dec^{-1})
Blank	134 ± 9	0.52 ± 0.03	184 ± 6	515 ± 17
0.001 M	184 ± 7	1.07 ± 0.04	109 ± 9	513 ± 15
0.010 M	275 ± 10	1.32 ± 0.04	208 ± 11	388 ± 9
0.100 M	404 ± 12	3.92 ± 0.06	361 ± 18	176 ± 11

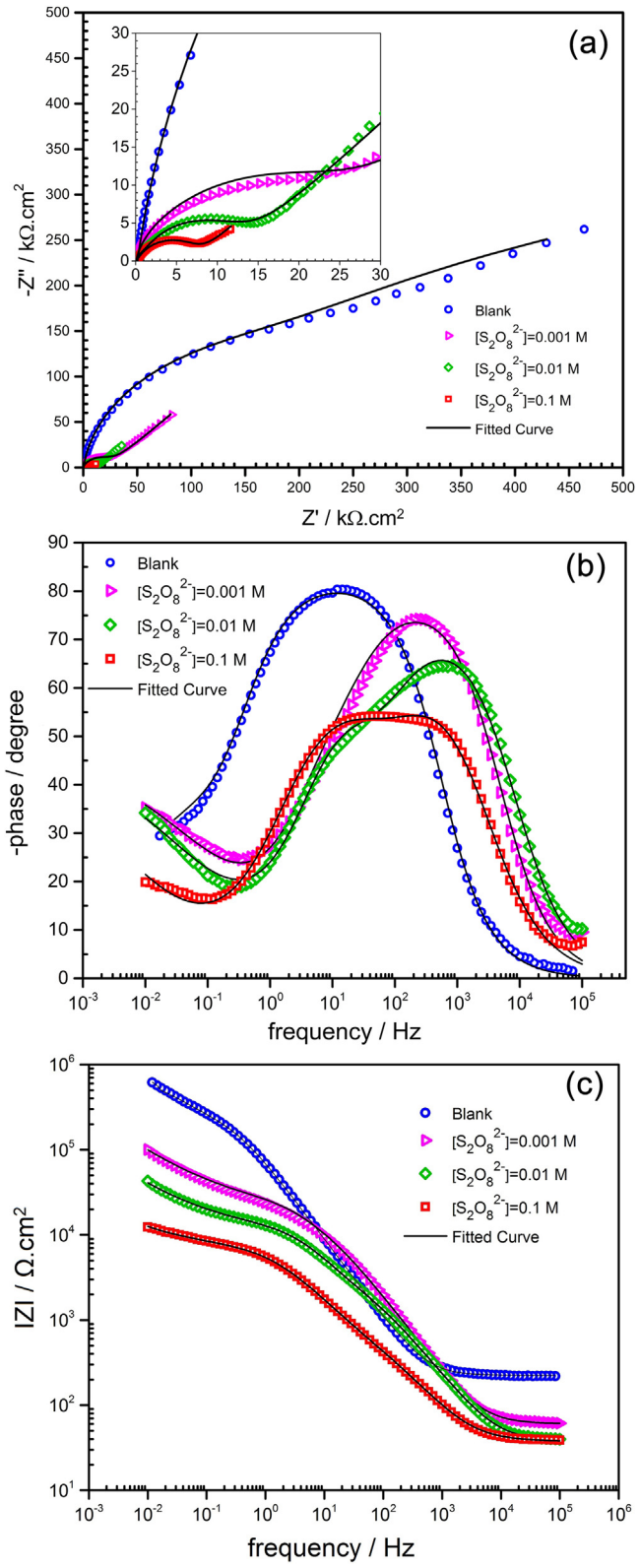

Fig. 4. Nyquist (a), Bode phase (b) and Bode magnitude (c) plots of chalcopyrite for different concentrations of peroxydisulfate in 0.5 M H_2SO_4.

increase in current density can be seen and passive layer destruction happens at potentials higher than 760 mV vs. SCE for all concentrations of oxidizer.

3.3. Electrochemical impedance spectroscopy (EIS)

Electrochemical impedance spectroscopy was employed to study the dissolution behavior of the chalcopyrite electrode in presence of different concentrations of peroxydisulfate ion in 0.5 M H_2SO_4. Experimental results of the EIS measurements on chalcopyrite electrode at OCP and related fitted curves are plotted in the form of Nyquist, Bode phase and Bode magnitude diagrams in Fig. 4(a–c). All spectra show a depressed type semicircle at high frequencies followed by a Warburg impedance at moderate and lower frequencies. The capacitive loop at high frequencies can be attributed to formation of chalcopyrite primary dissolution products on its surface due to initial immersion in the solution. Some authors have proposed that, at near open circuit potentials iron dissolves first and a nonstoichiometric copper-sulfur rich layer remains on the electrode surface [10,31–33]. More dissolution of iron forms thicker rich copper-sulfur layer which acts as a dense barrier and hinders further oxidation of the underlying $CuFeS_2$. According to this, the second loop of the Nyquist plot is considered as diffusional impedance of the passive layer.

In accordance with the equivalent circuit shown in Fig. 5, the solution resistance (R_s), double layer resistance (R_{dl}), constant phase element of the double layer (CPE_{dl}), Warburg diffuse element of the passive layer ($Warburg_p$), constant phase element of the passive layer (CPE_p) and passive layer resistance (R_p) were extracted and listed in Table 3. Also, n and P represent the CPE power and parameter, respectively. The plus and minus sign denotes standard deviation with three replicates determination. Table 3 demonstrates that diffusional transport restrictions of the passive layer has decreased at higher concentrations of peroxydisulfate ion because passive layer resistance is reduced. Another evidence for this claim is the total impedance of the system which has decreased obviously (reported values in Table 3) in presence of higher concentrations of oxidizer reagent (observed impedance module values in frequency 10^{-2} Hz in Fig. 4c). Also, values of CPE capacitance of the double layer were calculated using equation 3 [34]:

$$C_{dl} = (P_1)^{\frac{1}{n_1}}(R_{dl})^{\frac{1-n_1}{n_1}} \quad (3)$$

The significant increase in capacitance of the double layer with increasing peroxydisulfate ion concentration (Table 3) is attributed to demolition of the passive layer. An increase in local dielectric constant and thinning of the passive layer are possibly the reasons for the increase in capacitance of the double layer [35]. Moreover, the variation of n values can be attributed to the surface roughness changes. A meaningful decrease in n value at solution containing 0.1 M peroxydisulfate indicates severe attack of the exposed sample. In summary, the results of electrochemical impedance spectroscopy show that the total impedance of the system decreases with increasing the oxidizer concentration.

3.4. Mott-Schottky analysis

An ideal n-type semiconductor-solution interface follows the Mott-Schottky relationship below:

$$\frac{1}{C^2} = \frac{2}{\varepsilon\varepsilon_0 eN}\left(E - E_{fb} - \frac{kT}{e}\right) \quad (4)$$

where ε is the dielectric constant, ε_0 is the vacuum permittivity, e is the charge of an electron, N is the donor density, E is the applied potential, E_{fb} is the flat band potential, k is the Boltzman constant and T is the absolute temperature.

Chalcopyrite is an n-type semiconductor which shows little current flow by applying anodic polarization and this behavior remains up to breakdown potential. In addition, an interface of

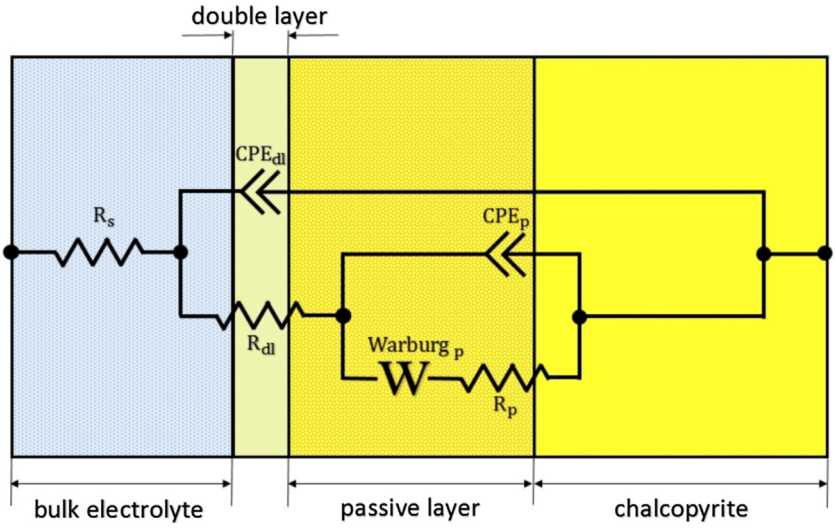

Fig. 5. Equivalent circuit for chalcopyrite in 0.5 M H_2SO_4 in presence and absence of peroxydisulfate.

Table 3
Electrochemical impedance spectroscopy parameters for chalcopyrite electrode in 0.5 M H_2SO_4 in presence and absence of peroxydisulfate.

	R_s (Ω cm^2)	CPE_{dl}		R_{dl} (Ω cm^2)	W_p (Ω s$^{-0.5}$)	CPE_p		Cdl (μF cm^{-2})	R_p (Ω cm^2)
		$P_1 \times 10^6$ (Ω^{-1} s$^n{}_1$)	n_1			$P_2 \times 10^6$ (Ω^{-1} s$^n{}_2$)	n_2		
Blank	223.7 ± 15	2.48 ± 0.09	0.92 ± 0.02	263400 ± 1782	40591 ± 820	10.01 ± 0.55	0.78 ± 0.02	1.958 ± 0.13	409540 ± 12350
0.001 M	60.5 ± 2	1.63 ± 0.12	0.89 ± 0.02	15296 ± 653	14702 ± 553	4.00 ± 0.17	0.82 ± 0.02	1.053 ± 0.07	11685 ± 565
0.01 M	37.8 ± 1	2.51 ± 0.19	0.86 ± 0.03	3359 ± 271	5566 ± 417	4.30 ± 0.14	0.83 ± 0.03	1.114 ± 0.06	9663 ± 411
0.1 M	37.5 ± 1	10.56 ± 0.73	0.80 ± 0.03	891 ± 82	1101 ± 68	17.15 ± 0.29	0.72 ± 0.02	3.384 ± 0.15	6845 ± 396

solution and n-type semiconductor should have positive slope on a Mott-Schottky plot [12]. In present study, Mott-Schottky analysis of chalcopyrite electrode at 1 kHz frequency in the potential range of 300 mV to 900 mV (vs. SCE) with amplitude of ±10 mV was conducted for different concentrations of peroxydisulfate ion. The results are presented in Fig. 5 together with potentiodynamic polarization curve of chalcopyrite electrode in presence of 0.1 M peroxydisulfate ion in background.

The Mott-Schottky curves show two distinct linear regions before and after 680 mV vs. SCE. These two linear regions are in accordance with depletion region of an n-type semiconductor [12]. At potentials lower than 680 mV, the linear behavior of Mott-Schottky plot could be interpreted as pseudo-passive behavior of the chalcopyrite as shown in the background of Fig. 6. Comparing four plots at each concentration of peroxydisulfate ion, it is obvious that the slope of Mott-Schottky curves and magnitude of C^{-2} have

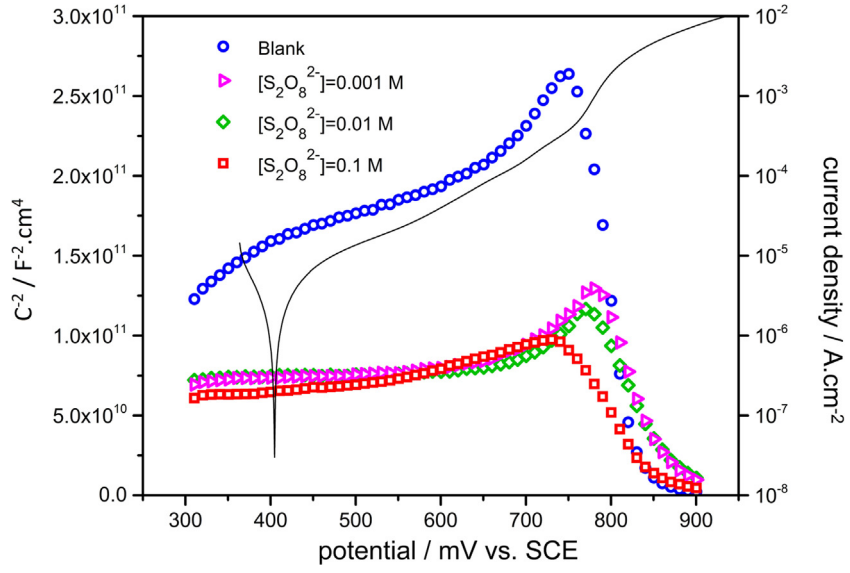

Fig. 6. Mott–Schottky plots for chalcopyrite electrode in 0.5 M H_2SO_4 in presence and absence of peroxydisulfate.

decreased at higher concentrations of the oxidizer. To explain the change in slopes and the capacitance of the chalcopyrite surface, our previous findings in Sec.'s 3.2 and 3.3 suggest that when peroxydisulfate ion is present in the solution, the chalcopyrite passive film semiconducting properties, and subsequently the electrochemical dissolution mechanism has changed. In the second linear region at potentials between 680 mV to 760 mV (vs. SCE), the slope of all curves is still positive but its magnitude

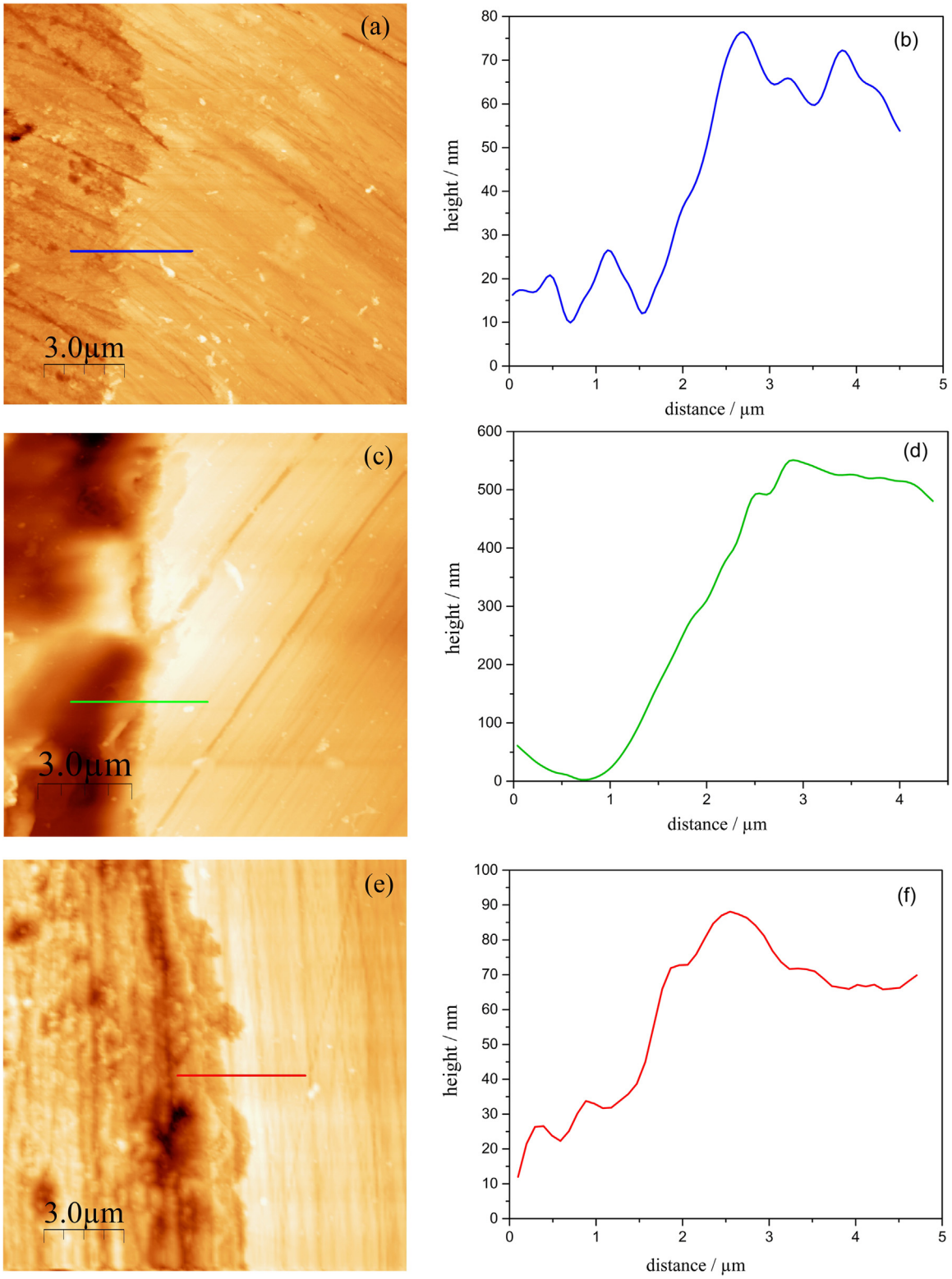

Fig. 7. Atomic force microscopy for chalcopyrite electrode. (a–b) 4 hours at 720 mV in 0.5 M H_2SO_4, (c–d) 4 hours at 720 mV in 0.5 M H_2SO_4 in presence of 0.1 M peroxydisulfate, (e–f) 4 hours at 820 mV in 0.5 M H_2SO_4.

has increased in comparison with the first region which could be related to significant growth of the passive film in this range of potential. At potentials greater than 760 mV vs. SCE, a sudden drop in Mott-Schottky plot is observed and the semiconducting behavior of chalcopyrite surface is in inversion region. In other words, accumulating of mobile holes on the chalcopyrite surface and dissolution of these holes increases the capacitance and current, simultaneously. In summary, the increasing peroxydisulfate ion concentration deteriorates the n-type properties of the chalcopyrite passive film resulting in an increase in current density.

3.5. Atomic force microscopy (AFM)

Fig. 7(a–f) shows topographical images of chalcopyrite samples including their line profiles which are obtained using test configuration in Fig. 1. Both attacked and non-attacked regions can be observed in a single AFM image. Atomic force microscopies were conducted under conditions that highlight the effects of peroxydisulfate ion and applied potential on chalcopyrite electrochemical dissolution. Previous experiments showed that the semiconductor chalcopyrite at potentials near 720 mV and 820 mV (vs. SCE) is in depletion and inversion regions, respectively. To check the influence of peroxydisulfate ion on chalcopyrite topographical changes, the electrode was held at 720 mV (vs. SCE) in presence and absence of 0.1 M peroxydisulfate ion for 4 hours. Severe attack with deeper formed ditch is clear in Fig. 7 (c–d) which proves an obvious progress in corrosion of the chalcopyrite surface in presence of 0.1 M peroxydisulfate ion in comparison with Fig. 7 (a–b). The image also confirmed the lower n value in Table 3 with higher surface roughness for solution with 0.1 M peroxydisulfate ion. Fig. 7 (e–f) is an evidence for changing in dissolution behavior of chalcopyrite at potentials higher than 760 mV (vs. SCE) because it is more corroded compared with Fig. 7 (a–b).

4. Conclusion

An investigation of the electrochemical behavior of chalcopyrite in 0.5 M H_2SO_4 in presence of peroxydisulfate ion in combination with analysis by atomic force microcopy added some useful information to the understanding of the chalcopyrite dissolution process under atmospheric conditions. Addition of peroxydisulfate ion accelerated the electrochemical dissolution of chalcopyrite in 0.5 M H_2SO_4 and polarization measurements proved this claim. Electrochemical impedance spectroscopy showed a depressed type semicircle at high frequencies followed by a Warburg impedance at moderate and lower frequencies. EIS measurements showed that presence of peroxydisulfate ion has decreased charge transfer resistance of the double layer and the total impedance of the system. Mott-Schottky analysis of chalcopyrite obeys an n-type semiconductor. Higher concentrations of peroxydisulfate ion weakens the n-type properties of chalcopyrite passive film and results in higher current densities at anodic polarization. Finally, atomic force microscopy directly evidenced that chalcopyrite surface severely corrodes in presence of peroxydisulfate ion compared with blank 0.5 M H_2SO_4.

Acknowledgments

Authors would like to appreciate the financial support from national Iranian copper company (NICICO) and Sarcheshmeh copper complex during the period that this research was conducted.

References

[1] M.E. Schlesinger, et al., Extractive metallurgy of copper, Elsevier, 2011.
[2] D. Dreisinger, Copper leaching from primary sulfides: Options for biological and chemical extraction of copper, Hydrometallurgy 83 (1) (2006) 10–20.
[3] H. Watling, The bioleaching of sulphide minerals with emphasis on copper sulphides—a review, Hydrometallurgy 84 (1) (2006) 81–108.
[4] G. Debernardi, C. Carlesi, Chemical-electrochemical approaches to the study passivation of chalcopyrite, Mineral Processing and Extractive Metallurgy Review 34 (1) (2013) 10–41.
[5] G. Yue, E. Asselin, Kinetics of Ferric Ion Reduction on Chalcopyrite and its Influence on Leaching up to 150 °C, Electrochimica Acta 146 (2014) 307–321.
[6] A. López-Juárez, N. Gutiérrez-Arenas, R. Rivera-Santillán, Electrochemical behavior of massive chalcopyrite bioleached electrodes in presence of silver at 35C, Hydrometallurgy 83 (1) (2006) 63–68.
[7] O. Solís-Marcial, G. Lapidus, Study of the Dissolution of Chalcopyrite in Sulfuric Acid Solutions Containing Alcohols and Organic Acids, Electrochimica Acta 140 (2014) 434–437.
[8] P. Velasquez, et al., A chemical: morphological, and electrochemical (XPS, SEM/EDX, CV, and EIS) analysis of electrochemically modified electrode surfaces of natural chalcopyrite (CuFeS2) and pyrite (FeS2) in alkaline solutions, The Journal of Physical Chemistry B 109 (11) (2005) 4977–4988.
[9] N. Hiroyoshi, et al., Synergistic effect of cupric and ferrous ions on active-passive behavior in anodic dissolution of chalcopyrite in sulfuric acid solutions, Hydrometallurgy 74 (1) (2004) 103–116.
[10] A. Ghahremaninezhad, E. Asselin, D. Dixon, Electrochemical evaluation of the surface of chalcopyrite during dissolution in sulfuric acid solution, Electrochimica Acta 55 (18) (2010) 5041–5056.
[11] A. Ghahremaninezhad, et al., A model for silver ion catalysis of chalcopyrite (CuFeS2) dissolution, Hydrometallurgy 155 (2015) 95–104.
[12] F. Crundwell, The semiconductor mechanism of dissolution and the pseudo-passivation of chalcopyrite, Canadian Metallurgical Quarterly 54 (3) (2015) 279–288.
[13] A. Ghahremaninezhad, D. Dixon, E. Asselin, Electrochemical and XPS analysis of chalcopyrite (CuFeS 2) dissolution in sulfuric acid solution, Electrochimica Acta 87 (2013) 97–112.
[14] T. das Chagas Almeida, et al., Electrochemical study of chalcopyrite dissolution in sulfuric, nitric and hydrochloric acid solutions, International Journal of Mineral Processing 149 (2016) 25–33.
[15] H. Zhao, et al., Electrochemical dissolution process of chalcopyrite in the presence of mesophilic microorganisms, Minerals Engineering 71 (2015) 159–169.
[16] J. Xiao, et al., The interaction of N-butoxypropyl-N′-ethoxycarbonylthiourea with sulfide minerals: Scanning electrochemical microscopy, diffuse reflectance infrared Fourier transform spectroscopy, and thermodynamics, Colloids and Surfaces A: Physicochemical and Engineering Aspects 456 (2014) 203–210.
[17] A. Ghahremaninezhad, D. Dixon, E. Asselin, Kinetics of the ferric-ferrous couple on anodically passivated chalcopyrite (CuFeS 2) electrodes, Hydrometallurgy 125 (2012) 42–49.
[18] N. Hiroyoshi, et al., Enhancement of chalcopyrite leaching by ferrous ions in acidic ferric sulfate solutions, Hydrometallurgy 60 (3) (2001) 185–197.
[19] H. Watling, Chalcopyrite hydrometallurgy at atmospheric pressure: 1. Review of acidic sulfate, sulfate-chloride and sulfate-nitrate process options, Hydrometallurgy 140 (2013) 163–180.
[20] M.D. Turan, H.S. Altundoğan, Leaching of chalcopyrite concentrate with hydrogen peroxide and sulfuric acid in an autoclave system, Metallurgical and Materials Transactions B 44 (4) (2013) 809–819.
[21] F.R.C. Pedroza, et al., Treatment of sulfide minerals by oxidative leaching with ozone, Mineral Processing and Extractive Metallurgy Review 33 (4) (2012) 269–279.
[22] S. Aydogan, G. Ucar, M. Canbazoglu, Dissolution kinetics of chalcopyrite in acidic potassium dichromate solution, Hydrometallurgy 81 (1) (2006) 45–51.
[23] S. Kariuki, C. Moore, A.M. McDonald, Chlorate-based oxidative hydrometallurgical extraction of copper and zinc from copper concentrate sulfide ores using mild acidic conditions, Hydrometallurgy 96 (1) (2009) 72–76.
[24] P. Canizares, et al., Electrochemical synthesis of peroxodiphosphate using boron-doped diamond anodes, Journal of the Electrochemical Society 152 (11) (2005) D191–D196.
[25] Merck Millipore. June 20, 2016; Available from: http://www.merckmillipore.com/INTL/en/product/Potassium-peroxodisulfate,MDA_CHEM-105092.
[26] A. Tsitonaki, B.F. Smets, P.L. Bjerg, Effects of heat-activated persulfate oxidation on soil microorganisms, Water research 42 (4) (2008) 1013–1022.
[27] Rankin D.W., CRC handbook of chemistry and physics, In: David R. Lide (Ed.). 2009.
[28] F. Dakubo, J.C. Baygents, J. Farrell, Peroxodisulfate assisted leaching of chalcopyrite, Hydrometallurgy 121 (2012) 68–73.
[29] M.A. Amin, et al., Polyacrylic acid as a corrosion inhibitor for aluminium in weakly alkaline solutions. Part I: Weight loss, polarization, impedance EFM and EDX studies, Corrosion Science 51 (3) (2009) 658–667.
[30] M. Behpour, et al., The effect of two oleo-gum resin exudate from Ferula assa-foetida and Dorema ammoniacum on mild steel corrosion in acidic media, Corrosion Science 53 (8) (2011) 2489–2501.

[31] D. Nava, I. González, Electrochemical characterization of chemical species formed during the electrochemical treatment of chalcopyrite in sulfuric acid, Electrochimica Acta 51 (25) (2006) 5295–5303.
[32] D. Nava, et al., Surface characterization by X-ray photoelectron spectroscopy and cyclic voltammetry of products formed during the potentiostatic reduction of chalcopyrite, Electrochimica Acta 53 (14) (2008) 4889–4899.
[33] Q. Yin, et al., Surface oxidation of chalcopyrite (CuFeS2) in alkaline solutions, Journal of the Electrochemical Society 147 (8) (2000) 2945–2951.
[34] B. Hirschorn, et al., Determination of effective capacitance and film thickness from constant-phase-element parameters, Electrochimica Acta 55 (21) (2010) 6218–6227.
[35] H.H. Hassan, Perchlorate and oxygen reduction during Zn corrosion in a neutral medium, Electrochimica acta 51 (26) (2006) 5966–5972.